TuneTag: Impedance-Matched RFID Tag for Long-Range and Reliable Battery-Free Sensing

Ishan Bansal, *Member, IEEE*, Nagarjun Bhat, *Graduate Student Member, IEEE*, Harine Govindarajan, Agrim Gupta, and Dinesh Bharadia, *Senior Member, IEEE*

***Abstract*—While RFID has expanded to passive sensing, its adoption is limited by constrained range and challenges like data sparsity, temporal misalignment, phase ambiguity, and environmental interference. We introduce TuneTag, a passive sensing platform featuring a custom tag with a novel impedance-matched antenna for improved precision and range, alongside a low-complexity algorithm compatible with commercial RFID readers and ICs. This algorithm corrects timing and phase inconsistencies, enabling robust differential sensing. Our evaluations demonstrate that TuneTag achieves a 5× improvement in sensing accuracy, a 2.4× extended range, and reduces latency to sub-second levels, yielding a 5× improvement in response time over State of the Art systems. The system features a graphical user interface (GUI) for near real-time sensor output display. We developed an Augmented Reality (AR) smartphone app that detects sensors and overlays live camera feeds with real-time data.**

***Index Terms*—Impedance matching, passive sensing range, sensing accuracy, real-time sensing.**

I. Introduction

As DATA-DRIVEN automation redefines modern infrastructure, the widespread deployment of IoT sensors will drive the next wave of transformation in industrial and home automation. To support this shift at scale, sensing platforms must be cost- and energy-efficient, requiring minimal additional infrastructure for deployment. In this regard, RFID presents a compelling solution, offering a mature infrastructure, evolving form factors [1], and supporting low-cost, easily deployable tags. These advantages have spurred growing research into using RFID tags to sense force, temperature, moisture, and more [2], [3], [4], [5], [6]. While traditionally used for identification, adding sensing functionality to RFID tags introduces energy demands that limit sensing range and reliability. For example, early designs with integrated ADC-based sensors [7], [8] were phased out due to insufficient on-chip energy to support ADC operations.

More recently, a newer class of tags that tune their self-impedance via an integrated varactor to maximize on-chip RSSI (OC-RSSI) has gained both academic [9] and commercial [10], [11] interest. These systems sense by monitoring impedance changes at the antenna terminals in response to the target stimulus, which are then translated into discrete digital sensor codes. While these designs offer advantages over ADC-based approaches, their functionality is constrained by a narrow OC-RSSI operating window, a limited impedance tuning range, and high sensitivity to environmental changes affecting antenna impedance–making them impractical for passive sensing in the real-world.

Analog sensors can directly modulate the RFID carrier signal's phase or RSSI [12], but reliable performance in dynamic environments often requires a colocated reference tag [4], [5]. These setups are sensitive to angle of arrival variations due to the presence of two distinct radiation phase centers, leading to instability under changing conditions. To mitigate this, prior work has explored using a single antenna shared by two RFID ICs through isolated ports or orthogonal radiation modes [13], [14]. However, achieving sufficient isolation or modal separation typically requires electrically large antennas. Electrically small antennas, which are essential for compact and flexible RFID tags, do not support the spatial or modal separation needed for these configurations. **ZenseTag** [15] offers a compact solution that enables two ICs to share a single commercial RFID antenna using a Wilkinson Power Combiner. This configuration provides the necessary isolation while preserving a flexible form factor. However, each IC receives 3dB less power compared to a standard single IC tag, which limits the sensing range to $< 1m$. Additionally, impedance mismatches between the COTS RFID antenna, the 50Ω PCB, and the ICs reduce both range and the accuracy of differential phase and RSSI measurements.

At the signal level, these systems [12], [15], [17] implement differential sensing by comparing outputs from a reference and a sensor tag to cancel multipath effects in dynamic environments. However, this differential sensing approach comes with a caveat: since passive RFID tags cannot sense the channel, commercial readers like the Impinj R700 and ThingMagic Sargas [18] must individually query each RFID Integrated Circuit (IC) using a Slotted ALOHA protocol with a Q-algorithm to manage collisions, particularly in dense-tag environments [19], [20]. This creates a signal processing challenge: the phase and RSSI streams from the two differential ICs arrive at different times, with unpredictable offsets. These offsets depend on how much backscatter is received from each IC, which in turn is affected by the two-way signal attenuation unique to each tag. As a result, one IC may take longer to harvest energy before responding, while the other

Received 29 June 2025; revised 3 September 2025; accepted 20 September 2025. Date of publication 26 September 2025; date of current version 3 October 2025. *(Ishan Bansal, Nagarjun Bhat, and Harine Govindarajan contributed equally to this work.) (Corresponding author: Ishan Bansal.)*

The authors are with the Department of Electrical and Computer Engineering, University of California at San Diego, La Jolla, CA 92093 USA (e-mail: isbansal@ucsd.edu; nbhat@ucsd.edu; hgovindarajan@ucsd.edu; agg003@ucsd.edu; dbharadia@ucsd.edu).

Digital Object Identifier 10.1109/JRFID.2025.3614590

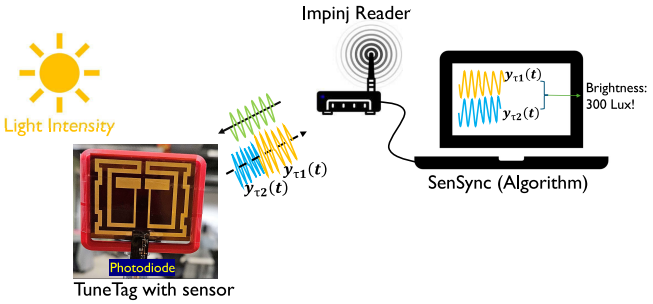

Fig. 1. TuneTag enables passive wireless sensing using an impedance-matched, sensor-integrable tag and a low-complexity decoding algorithm [16].

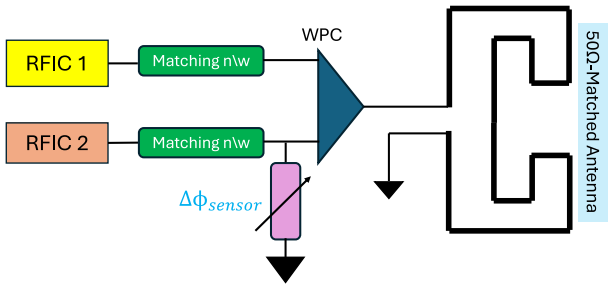

Fig. 2. TuneTag integrates a passive matching network and 50Ω antenna to improve energy transfer and differential sensing range.

may transmit multiple backscatter signals, leading to uneven time gaps between measurements. To ensure reliable sensor readings in such dynamic conditions–without relying on digital modulation–the reader must process the RSSI or phase data from both tags in a synchronized manner. These hardware and signal processing challenges pose a fundamental question: How can we enable accurate, low-latency passive analog sensing over practical ranges while maintaining a compact, cost-effective form factor?

To address this challenge, TuneTag proposes a two-pronged solution involving both **Hardware** and **Algorithm** as illustrated in Fig. 1

- *Hardware:*A uniform-impedance system that connects the sensor interface, antenna, and RFID ICs on a monolithic PCB.
  1) A new RFID antenna structure matched to the 50Ω input port of the Wilkinson Power Combiner, as shown in Fig. 2.
  2) A passive matching circuit to interface the RFID IC with the ZenseTag PCB, optimizing the match between the IC and 50Ω transmission lines from the Wilkinson Power Combiner (WPC) distribution ports, resulting in improved sensing range and more accurate differential Phase/RSSI measurements.
  3) A custom flexible sensing tag measuring just 40× 50 mm, printable and easily assembled at scale.
- *Algorithm:* A low-latency, low-compute time series matching algorithm.
  1) A sensing algorithm in SenSync [16] that resolves phase ambiguities and aligns time-shifted data from multiple ICs, enabling accurate differential sensing in real-world RFID applications.

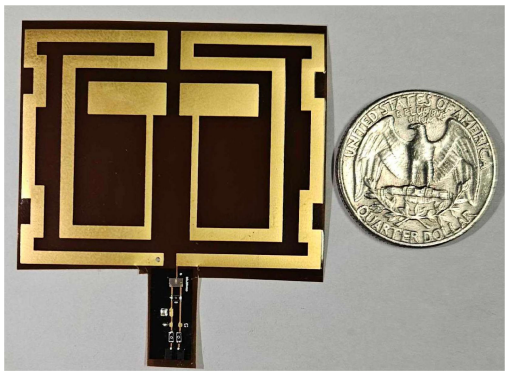

Fig. 3. Compact Form Factor: TuneTag measures just 40×50 mm (next to a US quarter for scale).

  2) A graphic user interface that can plot the sensor output in real-time which can even be overlaid on a camera-feed or Augmented-Reality (AR) as described in [21]

We evaluated TuneTag for sensing multiple modalities including known inductance, capacitance, and resistance (LCR) values, and demonstrated that within a specific range, it achieves measurement reliability comparable to wired instrumentation. Building on the **ZenseTag** [15] architecture and leveraging the **SenSync** [16] algorithm, TuneTag delivers notably improved performance: a **5x** improvement in sensing accuracy, a **2.4x** increase in range, and sub-second sensing latency on par with SenSync, resulting in a **5x** faster response time than other existing passive sensing systems.

II. Related Works

Ubiquitous, and passive environmental sensing has motivated the development of numerous tag-based sensor platforms, as seen in both academic literature and commercial products [22]. However, the lack of a ubiquitous energy source makes it challenging to read and transmit sensor data over meaningful ranges. Traditional digital-sensing topologies [2], [8] operate within a very limited power budget, due to significant energy consumption by ADCs and MCUs whose efficiency, despite significant research, remains fundamentally constrained [23]. This creates a major barrier to battery-free digital sensing. Alternative solutions, such as using photovoltaic or piezoelectric energy sources [24], [25], have been explored, but these require specific external conditions (such as sunlight or vibration). In environments without such sources (for example, indoors or in densely vegetated farms), these platforms cannot operate, limiting applicability.

An obvious choice in such scenarios, is harvesting energy carried by wireless signals since all sensing systems require a wireless carrier for data transmission. Thus RF energy harvesting, an inherent capability of passive RFID ICs, offers a promising route to achieve battery-free sensing. Recent works [4], [26] have utilized harvested RF energy for fully analog sensing, thus enabling both identification/tracking and additional sensing tasks. Expanding on this concept, [4], [27] demonstrate that multiple tags, even without direct sensor integration, can be used to infer physical properties such

TABLE I
COMPARATIVE ANALYSIS OF ANALOG SENSING TECHNIQUES USING RFID

Attribute	PV Sensing [31]	Co-located tags [4], [32]	This work
Universal Sensing Interface (different stimuli)	No	No	Yes
Robustness to wireless environment	Not evaluated	Poor	High
Commodity RFID compatible	No (needs USRP)	Yes	Yes
Battery-free	No	Yes	Yes
Prototype Evaluation	Wired (bench-top only)	Wireless	Wireless
Timing synchronization for switch	Reader-MSW Sync Required	No Sync	No Sync
Tag Modification	Significant	None	Moderate (new PCB)
Additional Implementation Cost	High	None	Low (flex-PCB+ WPC)

as soil moisture or material composition. However, these approaches face important limitations. Tags placed too closely may interfere with each other, leading to collisions [28], while increasing the distance between them alters the wireless channel and introduces phase errors due to variations in signal angle of arrival (AoA) [29]. As a result, determining optimal tag placement becomes a complex tradeoff. Similarly, other RFID-based sensing systems have used changes in impedance [3], [9], RSSI [12], and phase [6], [15] to measure environmental stimuli. Impedance-based sensing [9] is another alternative, but it requires careful matching of the sensor's impedance to the RFID IC and maintaining the on-chip RSSI within tight limits [30]. Additionally, impedance measurements are sensitive to tag-reader distance and may need frequent recalibration. If different conditions lead to similar impedance values, this method can also struggle with accurate identification [3]. Some studies have combined multiple parameters for sensing [17]. Although both RSSI and phase can be used for sensing, phase provides finer granularity and real-time sensitivity [6] compared to amplitude, making it a better parameter to measure different phenomena.

Despite these novel ideas, several key hardware and algorithmic shortcomings remain unaddressed in the literature.

(i) Algorithmic: While phase offers finer sensing resolution but poses significant implementation challenges on commercial off-the-shelf (COTS) RFID readers. These readers perform pseudo-random frequency hopping to reduce channel congestion [19], [20]. However, each channel transition introduces abrupt phase discontinuities, typically in multiples of π as noted in [15], [17]. These artificial phase jumps make it difficult to distinguish between environmentally induced phase changes and those caused by hopping [33], rendering phase an unreliable sensing parameter. To address this, [6] proposes tracking phase variation over short, stable intervals. While effective in static conditions, this approach breaks down in dynamic environments where channel conditions shift rapidly, such as with moving sensors. Recent single-antenna architectures [15], [17] aim to reduce sensitivity to multipath and channel variability by assuming a consistent backscatter channel. However, these systems rely on key assumptions:

- Concurrent reception and transmission from multiple RFID ICs.
- Synchronous alternation between IC responses.

In practice, these systems achieve read rates of about 100 RF ICs per second [15], [17]. By contrast, commercial readers like the Impinj R700 can handle 800–1000 RF ICs per second. Since differential sensing requires pairing responses from two ICs to produce a single measurement, current methods yield only about 50 sensory samples per second–well below the throughput capacity of modern readers. This highlights a significant under-utilization of existing RFID reader capabilities.

(ii) Hardware: While connecting two tags to a single phase center as in [15], [17] does alleviate the problem of ambiguous AoA and coupling, these designs rely either on the distinct polarizations of a large antenna [13] or a Wilkinson Power combiner to isolate the two tags. The former is incompatible with the desirable small form factor of RFID tags, while the latter loses energy due to impedance mismatches in the system. Passive sensing systems inherently suffer from RF path loss and the limited efficiency of electrically small antennas [34], making energy conservation a critical concern, particularly for miniaturized, RF-powered sensors. A comprehensive comparative analysis of various RFID based analog sensing approaches is provided in Tab. I.

In TuneTag, we address these limitations to maximize sensing range under strict energy and size constraints, and demonstrate our solutions via hardware implementation. In the following sections, we model these challenges and highlight the caveats of differential sensing using commercial RFID readers and tags. We then propose signal processing techniques to resolve phase ambiguities and fully leverage the reader's maximum read rate.

III. SYSTEM MODEL

The following section formalizes the energy and link-budget constraints of passive RFID tags, and explains their impact on sensing range and accuracy. We also formalize the design constraints that drive the algorithm design derived from Sensync [16].

A. Energy Constraints of a Commercial Passive RFID Tag

The read range of a passive RFID tag relying on harvested energy can be estimated using the Friis equation [35]:

$$r = \frac{\lambda}{4\pi}\sqrt{\frac{P_t G_t G_r \tau}{P_{\text{th}}}} \tag{1}$$

Here, $\mathbf{r}$ is the read range (in meters), $\mathbf{P_t}$ is the transmitted power (in watts), $\mathbf{G_t}$ is the transmit antenna gain, $\mathbf{G_r}$ is the tag antenna gain (often set to 1), τ is the power transmission coefficient, and P_{th} is the chip's threshold activation power.

The coefficient τ accounts for impedance mismatch between the RFID IC and antenna, and is given by:

$$\tau = \frac{4R_c R_a}{|Z_A + Z_C|^2} \tag{2}$$

where $Z_C = R_C + jX_C$ and $Z_A = R_A + jX_A$ are the chip and antenna impedances, respectively. Ideally, conjugate matching ($Z_C = Z_A^*$) yields $\tau = 1$, which ensures maximum power transfer and read range. However, in designs such as [15], where a sensing PCB with a 50Ω microstrip line is attached to a commercial RFID antenna, this mismatch results in suboptimal energy transfer.

B. Loss of Signal Strength in Differential Sensing

As discussed in Section I, reliable sensing with a dynamic channel often requires an additional RFID IC as a reference. Previous methods typically use one of two approaches:

1) Two Tags Using Dual Polarization: Losses due to polarization mismatch are sometimes overlooked since most commercial tags are electrically small and linearly polarized. Some works use dual-polarized patch antennas, powering two ICs via orthogonal modes. Assume the RFID reader transmits a right-hand circularly polarized (RHCP) wave, whose forward-propagating electric field is:

$$\vec{E}_{\text{RHCP}}(z,t) = E_0\big(\hat{x}\cos(kz-\omega t) + \hat{y}\sin(kz-\omega t)\big) \tag{3}$$

The electric fields exciting the two ICs are only half of the total incident field:

$$E_x = E_0\cos(kz-\omega t), \quad E_y = \pm E_0\sin(kz-\omega t) \tag{4}$$

$$|\vec{E}|^2 = |E_x|^2 + |E_y|^2 = E_0^2 \quad \Rightarrow \quad P_x = P_y = \frac{1}{2}P_{\text{CP}} \tag{5}$$

Each tag receives only half the incident power (a 3 dB loss). Moreover, as discussed in Section II, these tags' highly directive patterns perform poorly in non-line-of-sight settings–the typical case for sensing.

2) Dual Tags Using Wilkinson Power Combiner: Another approach is to isolate the two ICs using a Wilkinson power divider [15], [17]. Here, the received signal is split equally, so each IC also receives $\frac{1}{2}P_{\text{CP}}$, resulting again in a 3 dB loss. According to Eq. (1), this further reduces sensing range.

Additionally, some designs (e.g., "ZenseTag") use ICs with impedance $Z_L = 22 - j195\,\Omega$, which mismatches with the system impedance ($Z_0 = 50\,\Omega$). The resulting mismatch loss can be calculated as:

$$\text{Mismatch (dB)} = -10\log_{10}\Big(1-|\Gamma|^2\Big), \quad \Gamma = \frac{Z_L - Z_0}{Z_L + Z_0} \tag{6}$$

This leads to about a 10 dB loss, substantially degrading sensor range. We address these two-stage mismatch problems in TuneTag by developing a matching network and a 50Ω matched RFID antenna.

C. RFID Reader Operation

As discussed in SenSync [16], RFID readers–such as the Impinj R700–process parameters like RSSI, phase, and operating frequency. SenSync notes that these readers must comply with FCC regulations based on the EPC UHF Gen2v3 protocol [19], which restricts channel usage to avoid congestion [20]. In the U.S., readers operate from 902 MHz to 928 MHz, divided into 50 channels [20]. SenSync highlighted that frequency hopping (switching channels about every 200 ms) distributes use across the spectrum, but introduces unpredictable phase artifacts that complicate downstream processing.

D. Constraints on Differential Sensing

SenSync identified that EPC protocol-compliant readers communicate using framed Slotted ALOHA [19], [20]. Each tag transmits in a randomly assigned slot, making reads sequential and introducing time lags (δt) between IC responses. Fluctuations in energy harvesting, as well as reader protocol timing, can cause some ICs to transmit more frequently than others. According to SenSync, these timing differences degrade the reliability of differential sensing, since signals representing the same physical stimulus may be out of sync. Furthermore, SenSync observed that if the reader does not estimate the tag population, it defaults to a 16-slot frame, potentially wasting time in underpopulated systems [36]. Abrupt π phase jumps from channel hopping also interfere with interpreting meaningful sensory data.

E. Addressing System Challenges

To address these issues, SenSync proposed that ambiguous π phase jumps, introduced during frequency switching, require differentials to be computed only within samples from the same frequency channel. Combined with a slow typical sample rate (about 50 samples/s [15], [17]), and a 200 ms channel dwell time [20], SenSync found that only around 10 usable samples could be obtained per channel per interval. They also noted that data sources may transmit unevenly; for example, one IC might produce 7 samples while another produces 3, with only overlapping periods (in this case, 3 values) usable for differential analysis.

Therefore, SenSync concluded that a longer time window is required to gather enough samples for accurate measurement. While these systems are often described as "real-time," SenSync highlighted that, in practice, they require a 5–10 second window to reliably report sensor readings–a significant latency that undermines true real-time operation.

By addressing these constraints, SenSync demonstrated that TuneTag enables the next generation of RFID-based sensing, offering improved accuracy and performance even in dynamic and challenging environments.

IV. Design

In this section, we present the steps taken to design the TuneTag platform to enhance sensing range and overcome the limitations identified earlier. The design follows a two-step impedance standardization process: first, creating a matching network to match the IC for maximum power transfer, and second, designing an antenna that is matched to the transmission line impedance.

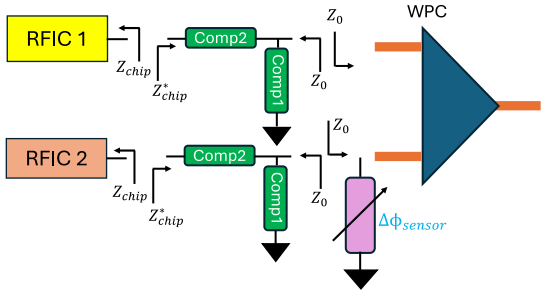

Fig. 4. Impedance matching to improve energy delivery to RFID [37].

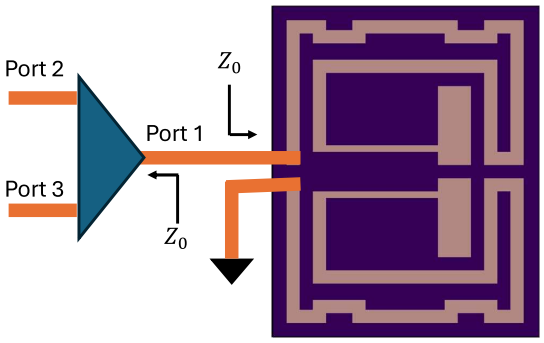

Fig. 5. Antenna impedance matched to 50Ω to maximize energy transfer.

A. Matching Network Design

To maximize the energy delivered to the RFID ICs, we use conjugate impedance matching–a standard technique for matching RFID ICs with electrically small tag antennas [35]. Transmission lines connected to Ports 2 and 3 of the Wilkinson Power Combiner (WPC) are designed for $Z_0 = 50\Omega$. A simple two-component matching network ensures the IC sees its conjugate matched impedance (Z^*_{chip}), while the rest of the system maintains a 50Ω load, minimizing reflection loss.

Simulations were run in Keysight Advanced Design System (ADS) with the load impedance set to Z^*_{chip} (i.e., $22+j195\,\Omega$). Based on the results, a two-capacitor network was selected (Comp1 = 3.8 pF, Comp2 = 1.0 pF), moving the impedance point to the center of the Smith chart. This matching circuit was then included in Ansys HFSS simulations together with the antenna to confirm its impact. Some energy is inevitably lost in the matching network, resulting in a 4 dB improvement (versus a theoretical 10 dB, see Fig. 10(a)). Nonetheless, the received RSSI from the RFID ICs is approximately 6 dB higher than without impedance standardization.

B. Antenna Design

The second step of impedance standardization in TuneTag is antenna design. Unlike typical RFID tags, which are conjugately matched to the IC [35], TuneTag enforces a system impedance of 50 Ω at the WPC ports. Traditional antenna designs are unsuitable due to mismatch (Section III). We therefore designed a novel, electrically small, omnidirectional antenna matched to 50 Ω at its input, as shown in Fig. 5. Our antenna is single-ended since the WPC only has one port. The other terminal connects to system/RF ground, shared by the PCB and all components. The antenna design was validated using Ansys HFSS simulations before fabrication as seen in Fig. 7.

C. TuneTag Fabrication

As discussed in Section I, TuneTag is designed for easy deployment, low cost, and scalability. We fabricated the tag on a 4 mil (0.1016 mm) thick flexible polyimide substrate ($D_k = 3.2$), making it suitable for applications such as soil moisture or in-shoe force sensing. The PCB can be manufactured using standard photolithography and etching, similar to rigid PCBs.

The total component cost is under $2. Future versions could leverage low-cost or biodegradable materials such as PET or paper, and simple, solder-free assembly. The platform is compatible with any 2-terminal sensor that changes its terminal impedance.

V. Addressing Limitations in Differential Sensing With TuneTag

Below, we summarize the design contributions of TuneTag that address the limitations of single-antenna differential sensing highlighted in Section III. Our hardware design improves on the architecture proposed in ZenseTag [15], but with major improvements in software derived from Sensync [16].

A. Addressing Temporal Mismatches

Earlier works [15], [17] did not address temporal mismatches caused by sequential tag reading, energy harvesting, and varying backscatter timing. As shown in Section VII, these mismatches resulted in large phase variation when analyzing unmatched sequences.

To solve this, an algorithm was developed in SenSync [16] that collects signal parameters from individual channels, temporally aligns them, and then computes phase differences. As detailed in SenSync, Dynamic Time Warping (DTW)–a dynamic programming method originally created for matching time series of varying speeds/lengths in speech recognition [38]–was used to align the data streams (see Fig. 6 and Algo. 1).

1) Mathematical Model of Backscatter from SST: This algorithm has been introduced in [16]. Consider the response that the reader receives from individual tags as independent channel (both RSSI and Phase) states h_1, h_2 for a given channel c:

$$h_1^c = |h_1^c|e^{-j\Phi_1^c}, \quad h_2^c = |h_2^c|e^{-j\Phi_2^c} \quad \ldots \Phi_1^c, \Phi_2^c \in (-\pi, \pi)$$

The differential amplitude (RSSI) and Phase can be represented as:

$$RSSI^c_{\text{diff}} = |h_1^c| - |h_2^c|, \quad \Phi^c_{\text{diff}} = \Phi_1^c - \Phi_2^c$$

The two sequences Φ_1 and Φ_2 represent phase values captured by the reader for the two tags over multiple channels. The input sequences are defined as:

$$\Phi_k = \{\Phi_k^1, \Phi_k^2, \ldots, \Phi_k^C\}, \quad k \in \{1, 2\},$$

where C is the number of channels, and $\Phi_k^c = \{\Phi_k^c(t_1), \Phi_k^c(t_2), \ldots, \Phi_k^c(t_N)\}$ is the phase sequence for channel c at different time instances $t_1, t_2, \ldots, t_N$.

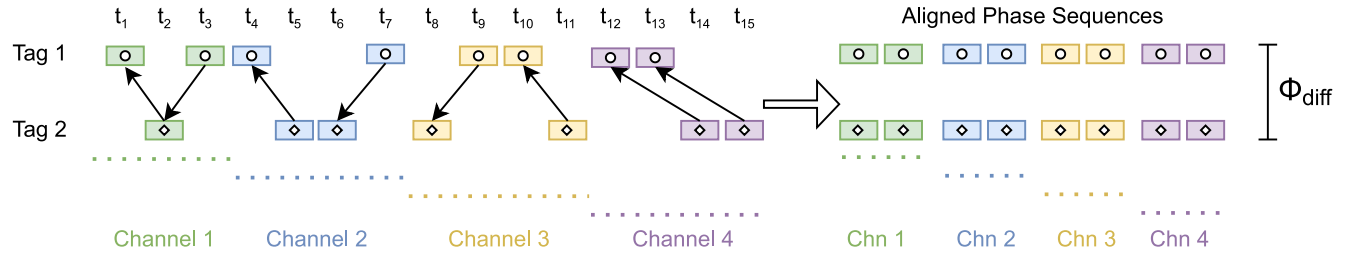

Fig. 6. Diagram showing data packets received from different RF ICs and their temporal alignment using DTW [16].

The number of channels, C has been fine-tuned based on hyperparameter optimization of the channel state for phase stability during the channel hops. Empirical data has shown that the arbitrary phase jumps of π happen approximately 15% of the time. Now, we have observed that having at least 3 stable channels is sufficient for our algorithm to correctly detect the response from the sensor and remove the effects of these arbitrary non-idealities. From binomial probability, 90% of 4 channel hops yield at least three reliable channels. Thus, we define each DTW time frame as 4 channels, corresponding to 0.8s of data, making our sensory response time 5× faster than current differential sensing algorithms [15], [17]. This aligns with stimulus variation and human perception rates.

The temporally misaligned phases can be represented as $\Phi_1(t+\tau)$,$\Phi_2(t)$ where τ represents the time shift introduced between the two streams in the same channel. Note that as the RFID reader hops channels, and communicates with the two tags, not necessarily in a sequential/deterministic order, the time-shift τ will also vary. Consequently, the objective is to align Φ_1 and Φ_2 by removing the shift τ over the minimum frame size (Algo. 1) within which the DTW algorithm computes the phase difference Φ_{diff}. The phase difference is given by:

$$\Phi_{\text{diff}}(t_i) = |\Phi_1(t_i) - \Phi_2(t_i)|, \quad \forall t_i \in W,$$

where W is the warping path obtained using DTW [1].

In Fig. 6, the left side of the diagram represents unprocessed input sequences from two tags (Φ_1 and Φ_2) across four channels:

$$\Phi_1 = \{\Phi_1^1, \Phi_1^2, \Phi_1^3, \Phi_1^4\}, \quad \Phi_2 = \{\Phi_2^1, \Phi_2^2, \Phi_2^3, \Phi_2^4\}.$$

Each sequence is time-indexed and contains noisy or misaligned data. Dynamic Time Warping is applied to each pair of sequences Φ_1^c and Φ_2^c per channel c, aligning the sequences and ensuring that the indices t_i match optimally.

After alignment, the processed output on the right side of the diagram represents the computed phase differences $\Phi_{\text{diff}}(t_i)$ for all aligned timestamps:

$$\Phi_{\text{diff}}^c(t_i) = |\Phi_1^c(t_i) - \Phi_2^c(t_i)|, \quad c \in \{1, 2, 3, 4\}$$

The final output is a consolidated matrix of Φ_{diff} values for all channels, ready for subsequent analysis.

As these sequences represent channel and stimulus effects, DTW was shown in SenSync to effectively align them despite time mismatches. This approach, solves the hidden challenges in single-antenna differential sensing. Additionally, the algorithm is not limited to phase and can be used for other signal parameters (RSSI, impedance), as noted by its authors.

Importantly, this deterministic approach does not require training data and can generalize to any environment without site-specific calibration, as highlighted in SenSync. Thus, according to its findings, TuneTag reliably addresses channel variability and enhances sensing robustness, which is detailed in the evaluations in Section VII.

TuneTag, as demonstrated by SenSync, enables robust differential sensing while dealing with common issues in commercial RFID readers (Section III). Since the algorithm works for multiple parameters, TuneTag serves as a universal

Algorithm 1 Dynamic Time Warping (DTW) [16]

Require: Two sequences $\Phi_1 = \phi_1(t_1), \phi_1(t_2), \ldots, \phi_1(t_N)$ and $\Phi_2 = \phi_2(t_1), \phi_2(t_2), \ldots, \phi_2(t_M)$

Ensure: The DTW distance and the optimal warping path W

Initialize the cost matrix D of size $N \times M$:
$D(0,0) = 0$
$D(i,0) = \infty$ for all $i > 0$
$D(0,j) = \infty$ for all $j > 0$
for each i from 1 to N **do**
  for each j from 1 to M **do**
    Calculate the cost $d(\phi_1(t_i), \phi_2(t_j)) = |\phi_1(t_i) - \phi_2(t_j)|$
    Update the cost matrix:

$$D(i,j) = d\big(\phi_1(t_i), \phi_2(t_j)\big) + \min\Big(D(i-1,j), D(i,j-1), D(i-1,j-1)\Big)$$

  end for
end for
Initialize the warping path $W = \{(N, M)\}$
Set $i = N, j = M$
while $i > 1$ or $j > 1$ **do**
  Find the direction of the minimum cost:

$$(i', j') = \arg\min\Big\{D(i-1,j), D(i,j-1), D(i-1,j-1)\Big\}$$

  Update $(i,j) \leftarrow (i', j')$
  Append (i,j) to W
end while
Reverse W to obtain the final warping path
return $D(N,M)$ and W

solution for RFID-based differential sensing. SenSync's work also showed that the increased throughput reduced sensing latency to sub-second levels, representing about an 80% improvement over existing state-of-the-art systems [15].

VI. Implementation

A. General Compute Specifications

As described in [16], SenSync was implemented as a software package built upon the hardware based on the design in ZenseTag [15]. The authors of SenSync further note that the complete system can be installed on any general-purpose computer running common operating systems [16].

The TuneTag software, as developed for SenSync, is a standalone Java application that uses the Impinj Octane SDK. This application features a graphical user interface (GUI) built with Java Swing, designed to display real-time sensor data and automatically detect nearby sensors. Users are also able to select specific sensors directly from the GUI. To demonstrate its compatibility with other programming languages, a Python program was also created for SenSync using the JPype library.

Performance of the SenSync system was evaluated on two distinct computing systems. As reported in [16], on a Windows 11 system with an Intel Core EVO i7-1355U CPU (3.7GHz peak clock speed), the application operated efficiently, utilizing less than 20% of the CPU's peak capacity and under 2 GB of memory. It also ran with similar effectiveness on an Ubuntu 20.04 machine, which has an Intel Core i7-1165G7 CPU (2.8GHz peak clock speed). These findings demonstrate TuneTag's robust cross-platform operability, as highlighted in SenSync. The code for the implementation can be found here: https://github.com/ucsdwcsng/SenSync [39].

B. Reader - Compute Interface

Most recently published works rely on Python-based open-source Low Level Reader Protocol (LLRP) libraries for interfacing the RFID reader with compute devices; however, these approaches are bottlenecked in terms of throughput due to limited packet sizes, resulting in significantly reduced sampling rates of 100 RF ICs (or 50 sensory samples) per second [15], [17]. Instead, in TuneTag's design as presented in SenSync, the Impinj R700 reader is interfaced with general-purpose compute devices using the Octane SDK provided by Impinj. A custom Java application was developed for SenSync using the existing SDK to handle RFID data acquisition and processing. It implements SenSync's algorithms for improved data interpretation and visualization.

Preset configurations were provided for the reader in SenSync, defining expected tag population and reader mode to set the correct frame size in the *Query* field [20]. Setting the correct reader mode optimizes resource allocation, allowing the reader to focus on decoding backscattered signals containing RFID parameters instead of evaluating its environment. Using this direct approach, SenSync reported that throughput was boosted to 800 RF ICs (or 400 sensory samples) per second.

By tailoring the software to the system's specific needs, SenSync created a robust platform for RFID data collection and analysis that enhanced throughput by 8× (as per Table II), enabling more efficient and accurate processing of complex RFID data streams.

TABLE II
Data Points Collected From SenSync and State of Art for Different Time Intervals [16]

Algorithm	1s	2s	5s	10s	30s	60s	Average
SenSync	771	1457	3607	7204	21259	42407	786 Hz
State of Art	114	199	478	947	2838	5744	99 Hz

C. Augmented Reality App

We tested our application using commercial off-the-shelf RFID tags and a separate commercially available Impinj R700 RFID reader. To demonstrate our algorithm's real-time capability, we developed an augmented reality Android App that can automatically detect sensors in the device's live camera feed or selected images, displaying sensed stimuli in real-time as was also shown in a short demo abstract in [21], [40]. Built on Google's MLKit library, the app runs on Android 9 (API level 28) or newer. It requires initial setup to link sensory tag identities with their purpose, which is then used to match objects and display live sensory data. Once configured, the app identifies objects in the camera view using object detection and optical character recognition (OCR), and displays corresponding sensor data directly within an augmented reality (AR) environment [21].

VII. Evaluation

We will now evaluate the performance of TuneTag in a real-world setting (laboratory) with ample multipath and show that we are able to achieve significantly better range and superior sensing accuracy.

A. Antenna Performance

The antenna was designed and simulated in Ansys HFSS. The simulation results show a reasonable match at around 915 MHz (center frequency of the UHF RFID band). The frequency response of the fabricated antenna was measured using a Keysight Vector Network Analyzer, while the radiation pattern was characterized using an anechoic chamber and a standard gain horn antenna.

The measured standalone antenna exhibits a resonance shifted upward to approximately 1100 MHz, representing a notable deviation from the intended design frequency. This shift is consistent with variability inherent to flexible Polyimide substrates, where fabrication processes such as thermal cycling and lamination can significantly alter the effective dielectric properties, effects that are difficult to capture precisely in simulation. While the resonance mismatch reduces the achievable sensing range compared to a perfectly matched design in the UHF RFID band, it does not affect the sensing accuracy of the system.

When the antenna is integrated with the PCB, however, the resonance shifts downward into the intended UHF RFID band. This tuning effect arises primarily from the influence of the PCB ground plane, which strongly affect both resonance and

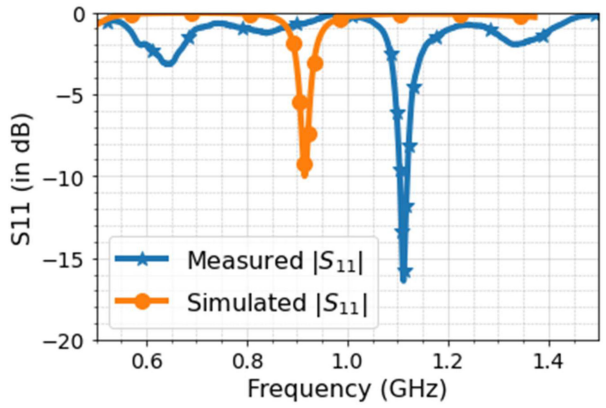

Fig. 7. Antenna characteristics: Simulated and measured S-parameters.

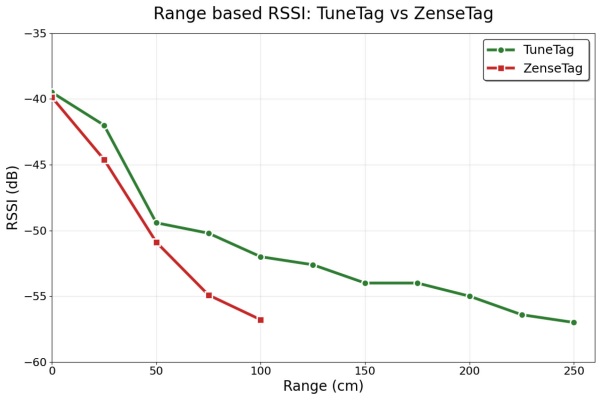

Fig. 8. Improved RSSI of TuneTag compared to prior work [15].

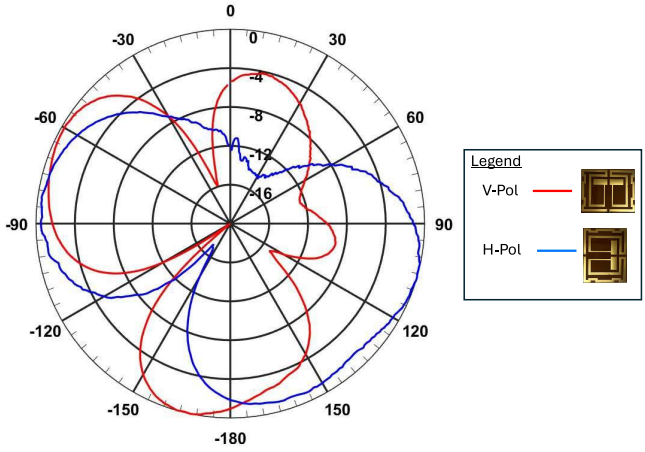

Fig. 9. Antenna radiation patterns for both H-pol and V-pol orientations.

radiation characteristics. Thus, although the fabricated antenna alone exhibits a resonance (matching) offset, the complete system operates effectively within the desired band once the PCB environment is included. An improved integrated antenna design in the future, where the RFID IC is explicitly modeled along with the antenna and PCB ground effects [41], could further mitigate such mismatches. The simulated and measured return loss (S_{11}) responses are shown in Fig. 7.

In contrast to the standalone antenna, the reflection coefficient (S_{11}) of the composite tag cannot be measured directly, as such a characterization would require a specially designed PCB with measurement ports substituting the RFID ICs. Consequently, to assess the performance of the composite tag consisting of the Wilkinson combiner, two RFID ICs, and the proposed antenna, we adopted a comparative evaluation based on the received signal strength indicator (RSSI). Specifically, the RSSI of the twin tag single antenna architecture with modified commodity RFID tag antennas reported in [15] is compared against that of the current design, measured across varying reader to tag distances (Fig. 8).

The measured radiation pattern of the fabricated RFID antenna is shown in Fig. 9. Patterns were recorded in both co-polarized (V-pol) and cross-polarized (H-pol) configurations relative to a reference horn. Comparable peak gain in both cases indicates negligible polarization selectivity, which is favorable for operation with right-hand circularly polarized readers. Localized nulls are observed in the measured patterns, attributed primarily to residual feed imbalance and secondarily to PCB ground asymmetry, but their impact is limited to narrow azimuthal regions when the antenna is connected to the differential sensing PCB.

B. Sensor Estimation Accuracy

The secondary goal of TuneTag is to improve the reliability of the sensing. Improving the SNR of the signal that reaches the RFID IC's will also ensure that the phase can be decoded more reliably at the reader end. To do this, we assembled a TuneTag without using any sensor to evaluate both the "differential-RSSI" and "differential-phase".

Past works [6], [15], [17] have relied on differential RSSI and Phase as the sensed metric, to measure quantities like contact (keyboard), force, soil moisture. The goal of this evaluation is to ascertain whether the impedance standardization process reduces the uncertainty in both parameters. Figures 10(a) and 10(b) show the standard deviation of both the measured RSSI values and the differential RSSI observed between the two RFID ICs. Notably, differential RSSI approaches the ideal value of **0 dB** and differential phase approaches **0**°.

C. Range Enhancement

To demonstrate the improvement in range achieved by TuneTag, we use the setup shown in Fig. 11(a), where the reader and the tag are mounted on tripods. The RFID antenna (Alien 9dBi gain) is fixed, while the tag bearing tripod is moved, till the tags are no longer read by the RFID reader software (ItemTest, which logs the tag RSSI and phase) on the HostPC. This helps us accurately measure the maximum range up to which the sensing platform will reliably function. Simultaneously, we also measure the sensing range of the state-of-the-art "ZenseTag". In order to ensure a fair comparison, both the platforms were evaluated without using any sensor. Also, TuneTag is measured without using matching network components, since the fabricated composite board (Antenna+PCB) had defective vias (large punchthrough). We

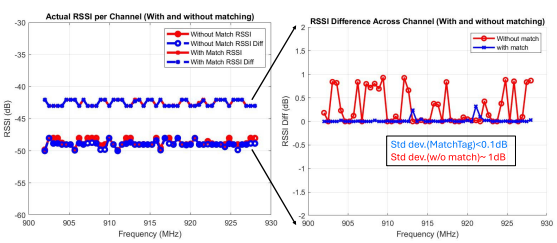

(a) Benchmarking Differential RSSI.

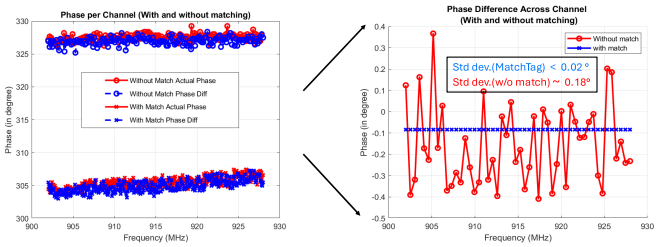

(b) Benchmarking Differential phase.

Fig. 10. Performance improvement in differential measurement due to improved matching between RFID IC and TuneTag PCB for (a) RSSI, and (b) phase.

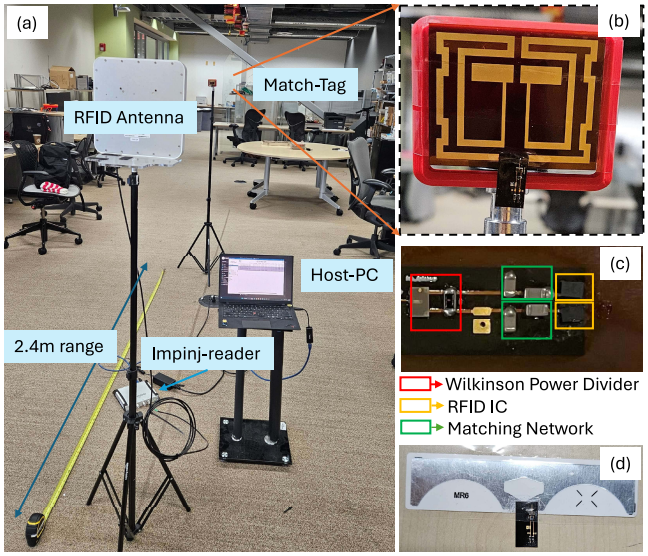

Fig. 11. (a) Setup to evaluate range of TuneTag. (b) TuneTag prototype using flexible polyimide substrate. (c) Matching network added to "ZenseTag" PCB. (d) "ZenseTag" prototype used for comparison.

notice from Fig. 11(a), that for TuneTag even without the tag-PCB matching, sensing range improved nearly **2.4**× to 2.4m compared to ZenseTag [15].

D. Measurement of RLC Components Using TuneTag

1) Measurement Methodology: We systematically varied known values of standard resistive, inductive, and capacitive components connected to the TuneTag system. For each component type (resistors, inductors, and capacitors), the differential signal (a derived signal parameter representing the tag's output response to the change in the component) was measured. These experimental measurements were then compared against simulated data which represents theoretical predictions derived from electromagnetic and circuit simulations, serving as the ideal benchmark as seen in Figs. 12(a),12(b),12(c).

2) Resistance Measurement: As shown in Fig. 12(a), the plot of Differential Amplitude versus Resistance demonstrates strong agreement between simulated values and evaluated results. One thing to note here is that while measuring resistance, differential RSSI proved to be the better metric showcasing the breadth of TuneTag in evaluating different signal parameters for sensing. This strong correlation confirms that TuneTag can accurately detect and quantify changes in resistance by observing variations in the differential amplitude of the backscattered signal. The minimal deviation between measured and simulated values underscores the effectiveness of TuneTag's impedance matching and signal processing in capturing subtle resistive variations with high fidelity, as amplitude is strongly influenced by resistance changes.

3) Inductance Measurement: Similarly, per Fig. 12(b), experimental validation for inductance shows that TuneTag is adept at measuring circuit inductance to a high degree of accuracy. The measured differential phase tracks the changes in inductance with precision and accuracy. This is crucial for applications sensitive to magnetic field variations or changes in inductive coupling, where phase provides a direct and highly sensitive indicator of the reactive component of the impedance arising from inductive changes.

4) Capacitance Measurement: The results for capacitance measurements, Fig. 12(c), further corroborate TuneTag's robust performance, again by focusing on the differential phase. Across a wide range of capacitive values (e.g., from picofarads to nanofarads), the experimental measurements show near-perfect alignment with both the simulated and estimated data curves. This high degree of conformity validates TuneTag's precision in detecting and quantifying capacitive changes. The ability to accurately sense capacitance is vital for numerous applications, including fluid level detection, proximity sensing, and material characterization.

The consistent and highly accurate alignment between experimental measurements, simulated data, and algorithmic estimations across resistance (using differential amplitude), inductance, and capacitance (using differential phase) proves that TuneTag is a versatile passive wireless sensing platform for most common sensor impedances.

E. Combining SenSync With TuneTag

To evaluate the technique proposed in SenSync [16], the authors of that work developed a Simulatory Stubbed Tag (SST) device, based on ZenseTag [15] but adapted for a rigid PCB implementation, as shown in the inset of Fig. 13. Unlike ZenseTag's sensor-impedance dependent phase modulation, SST utilizes a transmission line stub to introduce a fixed phase shift. The PCB incorporates two RFID ICs at known electrical lengths (calculated at effective wavelength λ_{eff} inside

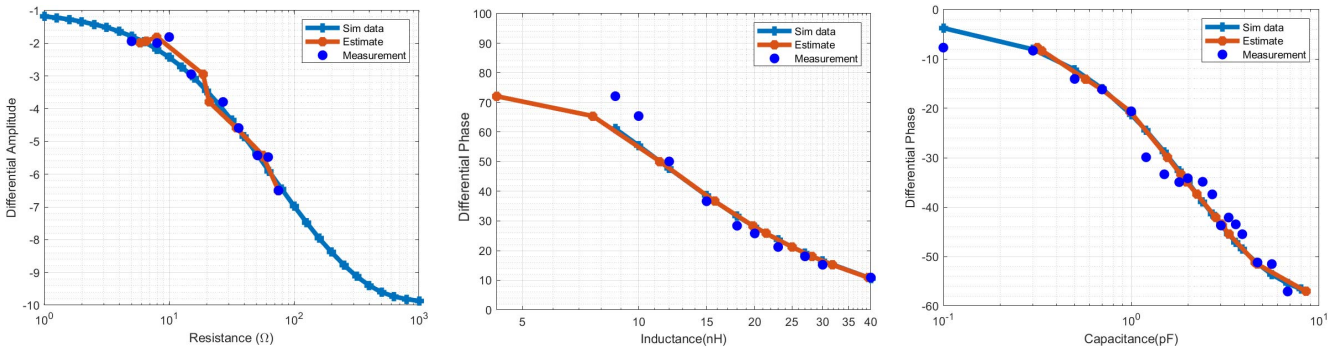

(a) Measurement of component resistance using TuneTag. (Differential RSSI).

(b) Measurement of component inductance using TuneTag. (Differential phase).

(c) Measurement of component capacitance using TuneTag. (Differential phase).

Fig. 12. Measurement of different passive components using TuneTag: (a) resistance, (b) inductance, and (c) capacitance.

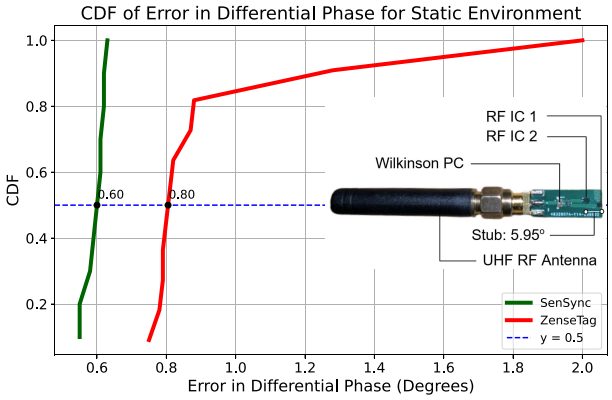

Fig. 13. CDF plot showing the error margins in static conditions. (Inset: Simulatory Stubbed Tag).

the substrate) from a shared antenna and Wilkinson Power Combiner, creating distinct path lengths.

This design induces a natural phase difference between incident and backscattered signals, enabling accurate phase-based sensing with a known ground truth. This calculated difference was 5.95° for each signal, resulting in a net phase difference of 11.9° for the backscattered signal, as confirmed using a Vector Network Analyzer (VNA). Using SST, SenSync compared its performance against ZenseTag [15]. This SST served as a benchmark to compare both methods' performance in two scenarios: optimal conditions without multipath interference, and challenging environments with significant multipath effects.

The authors of SenSync tested ZenseTag in dynamic conditions using their improved software and a simple differential technique on raw data, where they subtracted the phase of the reference without further processing, as described in [15], [16]. They evaluated both data collection methods using SenSync's DTW algorithm.

TuneTag, however, fuses the techniques given by ZenseTag and SenSync [15], [16] and significantly enhances the capabilities of the hardware by improving range **2.4**×. The results presented showed that accurate real-time sensing in dynamic conditions requires TuneTag's complete system.

1) Performance Under Static Conditions: In SenSync's evaluation under optimal conditions, the SST was positioned at 50cm from the RF antenna in an environment with static metallic and non-metallic objects nearby, but not in the Line of Sight (LOS) path.

The performance of both SenSync and ZenseTag was evaluated using the SST under these optimal conditions. Based on their observations, SenSync concluded that it provides significantly better accuracy and more precise results compared to ZenseTag. Fig. 13 from SenSync reveals that the median error in computing phase difference is 0.2° lower when using the algorithm proposed compared to the one suggested in [15].

2) Performance Under Dynamic Conditions: For the dynamic scenario in SenSync, significant disturbances were introduced in the LOS path, including moving people. Additionally, the SST was vigorously moved laterally relative to its platform.

Experimental Setup for Dynamic Movement Test:

To assess the system's resilience to localized tag movement while minimizing radial velocity effects, the tag underwent controlled oscillatory motion.

Movement Parameters: The SST was vigorously shaken back-and-forth, mimicking bottle-shaking:

- Average Speed: $\approx$ 1 m/s
- Peak Speed: Up to 2 m/s
- Type: Oscillatory, linear, within a constrained plane.

Rationale behind the movement restrictions: The shaking was strictly confined to the plane of the reader antenna's main radiation lobe. This ensured:

- *Consistent Tag-Antenna Distance:* Minimized direct physical distance changes.
- *Mitigated Radial Doppler Effects:* With motion perpendicular to the LoS ($\theta = 90°$), the radial velocity component ($v_r = v \cdot \cos(\theta) = 0$) was negligible. This isolated the system's performance from Doppler-induced phase distortions, allowing focus on temporal misalignments.

SenSync individually evaluated ZenseTag under these real-world conditions, focusing on their data collection and algorithmic capabilities. Specifically, ZenseTag was tested with SenSync's channel-wise DTW algorithm (Section V-A) and with their improved data collection technique (Section VI-B), which was equivalent to evaluating ZenseTag without the DTW algorithm. This approach demonstrated the independent impact

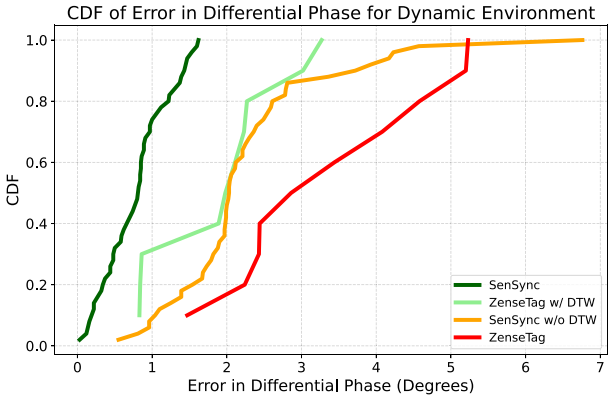

Fig. 14. CDF plot showing the error margins in dynamic conditions.

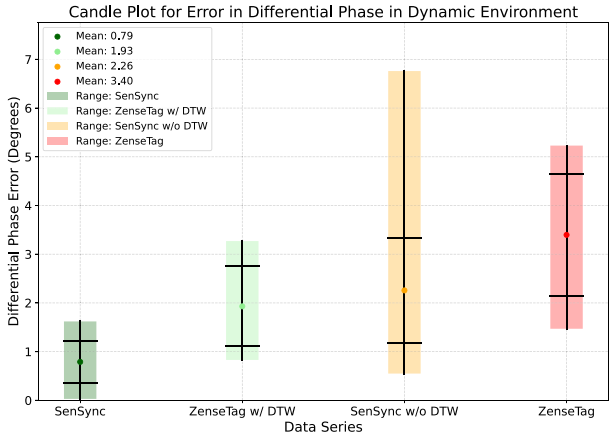

Fig. 15. Illustration of the range and variability in error in dynamic conditions.

of SenSync's design enhancements and detailed the optimal method for differential sensing.

SenSync achieves the lowest error, as shown in Fig. 14, with each individual enhancement also contributing significant improvement. It demonstrated substantial accuracy gains in measuring true differential phase. Under harsh simulation conditions, median error was only 0.79°, marginally higher than the 0.6° observed in static conditions Section VII-E1. ZenseTag with DTW, although a distant second, demonstrated DTW's effectiveness in matching time sequences for each channel and managing EPC protocol [19] constraints. Furthermore, SenSync's findings showed that omitting DTW matching (representing a throughput-enhanced ZenseTag) improved overall error but led to a more sporadic spread of values due to the absence of temporal sequence alignment.

The variability in readings for each experiment was also studied in SenSync, as seen in Fig. 15. As indicated by the dark green bar in their findings, SenSync outperformed others with lower error, reduced variability, and improved consistency. Its higher throughput (Table II) enabled sub-second stimulus resolution, achieving a 5× improvement over existing methods [3], [6], [15], [17]. Under these controlled planar oscillations, the system demonstrated exceptional stability and accuracy in differential phase measurements. This robust performance is attributed to effective radial Doppler mitigation, enabling SenSync's algorithm to address phase variations from sequential reads and non-radial interferences. Thus, TuneTag has been demonstrated to have significantly improved range, robustness and reliability compared to state-of-the-art.

F. Evaluation With Commercial Sensors

We also developed an Android application, as seen in Fig. 16, that detects sensors in a live camera feed or still images, augmenting them with real-time sensory values [21]. This application, as described in TuneTag, combines object detection with real-time sensory data acquisition, transforming phones into sensor hubs. As a result, users can remotely monitor metrics like soil moisture or container fill levels without physical presence. This technology, presented in [21], redefines remote sensing, making it accessible and user-friendly for everyday applications, from kitchen shelves to garden pots, enabling effortless and intelligent monitoring of one's environment.

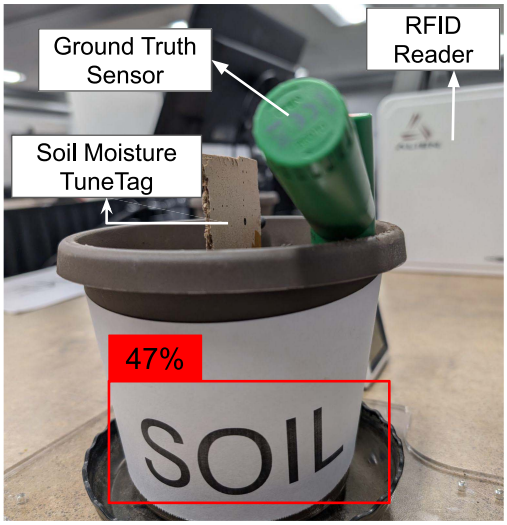

Fig. 16. TuneTag's AR Smartphone App: Visualizing Sensing in Real-time.

G. Overall Significance and Implications

These comprehensive validations indicate several key strengths:

1) *Adaptive Impedance Sensing:* TuneTag's ability to intelligently leverage the most sensitive signal parameter–differential amplitude for resistive changes and differential phase for reactive changes–demonstrates an effective approach to generalized impedance sensing. This is crucial because many physical phenomena (e.g., pressure, strain, humidity, material composition) can be transduced into changes in R, L, or C.
2) *Confidence in System Design:* The near-perfect alignment validates the entire TuneTag design, including the novel impedance-matched antenna, the passive tag's integration, and the sophisticated algorithms for signal processing and estimation. It confirms that the system behaves precisely as predicted by theory across both resistive and reactive domains.

3) *Reliability and Robustness for Applications:* The high prediction accuracy across diverse conditions indicates that TuneTag can provide consistent and precise data for battery-free passive sensing in varied environments.
4) *Foundation for Complex Sensors:* By accurately sensing R, L, and C using their most sensitive indicators, TuneTag lays the groundwork for seamless integration with a wide array of existing RLC-based passive sensors, simplifying their deployment and enabling miniaturized, battery-free solutions.

VIII. Conclusion

In TuneTag, we demonstrate that standardizing impedance across the differential sensing platform significantly enhances both range and accuracy. By using a novel RFID antenna with a 50Ω terminal and matching the RFID ICs to this common impedance, we enable practical, long-range passive sensing.

Wireless, battery-free solutions for ubiquitous remote sensing face numerous challenges, particularly in multipath-rich environments with static and non-static objects and people. We presented TuneTag with SenSync, an algorithm designed to address real-world non-idealities through a theoretical approach. Being a deterministic algorithm, SenSync requires no pre-training or post-deployment recalibration, making it suitable for any environment. We demonstrate this by developing a GUI that can capture and visualize real-time sensory outcomes, offering an intuitive model for RFID-based sensing.

TuneTag serves as a universal solution for RFID-based differential sensing, applicable to phase, RSSI, or impedance as sensing mechanisms. The current operation of TuneTag is constrained by sensor speed. Since we define the DTW time frame based on limitations imposed by commercial RFID readers, we are restricted to detecting stimuli that do not change more rapidly than the frame size. Another potential limitation is the use of handheld RFID readers. While TuneTag can account for tag movement, all our experiments have involved stationary readers.

As RFID readers improve in size, computing power, and become free of the arbitrary phase jumps introduced during frequency hopping, TuneTag can become more powerful. This advancement could potentially enable truly ubiquitous passive sensing, achieving the long-sought deploy-and-forget paradigm in remote sensing.

Future Work

A. Antenna Pattern Nulls

We note that the radiation pattern of the fabricated antenna exhibits certain null, which can create blind spots in its field of view specifically close to range limits. In these directions, the tag may fail to receive communicate with the reader, potentially leading to inconsistent tag reads or reduced communication reliability.

Future research can focus on refining the antenna design to minimize or eliminate these pattern nulls, thereby improving angular coverage and ensuring more uniform performance regardless of tag orientation or placement. Additionally, further tuning of the antenna geometry and material properties could enhance impedance matching, leading to more efficient power transfer between the antenna and RFID IC and ultimately extending the effective read range of the tag. Furthermore, in two-way backscatter based sensing, the key bottleneck is often the sensitivity of the RFID IC itself [37]. The uniform impedance tag idea presented in this work could support sensing at even longer ranges as the sensitivity improves.

B. Fabrication Complexity and Cost

The designed PCB is fabricated using a flexible polyimide substrate and requires manual soldering of key components, including the matching network, Wilkinson Power Combiner (WPC), and RFID ICs. While effective for prototyping and performance validation, this fabrication process introduces complexity and limits scalability for mass production.

Future research could explore simplifying the assembly process by adopting manufacturing techniques that are more compatible with large-scale production. For instance, using wet-inlay RFID ICs, where chips are pre-mounted on flexible substrates–along with printed or adhesive-based passive components, could eliminate the need for soldering altogether. This would pave the way for cost-effective, roll-to-roll fabrication of flexible sensing tags suitable for widespread deployment.

C. Tag Environment

We acknowledge that even with the use of a reference tag as in [15], environmental factors can still pose challenges, particularly when the antenna itself becomes significantly detuned by its surroundings. This issue is especially pronounced for RFID antennas, which are electrically small and typically lack a metallic ground plane (to preserve efficiency), making them highly susceptible to detuning when placed near metallic objects or reflective surfaces.

D. Impact of Radial Motion

While valuable, this test's planar restriction did not include significant radial tag motion. Future work is needed to quantify the impact of substantial Doppler frequency shifts, inherent in unconstrained tag movements, on differential phase stability and accuracy, and explore mitigation strategies for these complex scenarios.

References

[1] "EM45 Series | Zebra." 2025. Accessed: Mar. 27, 2025. [Online]. Available: https://www.zebra.com/us/en/products/mobile-computers/handheld/em45-series.html
[2] R. Menon, R. Gujarathi, A. Saffari, and J. R. Smith, "Wireless identification and sensing platform version 6.0," in *Proc. 20th ACM Conf. Embedded Netw. Sens. Syst.*, 2023, pp. 899–905. [Online]. Available: https://doi.org/10.1145/3560905.3568109
[3] E. Shen, W. Yang, X. Wang, S. Mao, and W. Bin, "TagSense: Robust wheat moisture and temperature sensing using a passive RFID tag," in *Proc. IEEE Int. Conf. Commun.*, 2022, pp. 1617–1622.
[4] J. Wang, L. Chang, S. Aggarwal, O. Abari, and S. Keshav, "Soil moisture sensing with commodity RFID systems," in *Proc. 18th Int. Conf. Mobile Syst. Appl. Services*, 2020, pp. 273–285. [Online]. Available: https://doi.org/10.1145/3386901.3388940
[5] W. Sun and K. Srinivasan, "Healthy diapering with passive RFIDs for diaper wetness sensing and urine pH identification," in *Proc. MobiSys*, 2021, pp. 188–201. [Online]. Available: https://doi.org/10.1145/3458864.3466870

[6] A. Gupta et al., "ForceSticker: Wireless, batteryless, thin & flexible force sensors," *Proc. ACM Interact. Mob. Wearable Ubiquitous Technol.*, vol. 7, no. 1, p. 13, Mar. 2023. [Online]. Available: https://doi.org/10.1145/3580793

[7] "AMS SL900A EPC Gen2 RFID dry-inlay tag interface." Accessed: Aug. 27, 2025. [Online]. Available: https://ams-osram.com/products/interfaces/sensor-interfaces/ams-sl900a-epc-gen2-sensor-tag

[8] J. R. Smith, A. P. Sample, P. S. Powledge, S. Roy, and A. Mamishev, "A wirelessly-powered platform for sensing and computation," in *Proc. 8th Int. Conf. Ubiquitous Comput.*, 2006, pp. 495–506. [Online]. Available: https://doi.org/10.1007/11853565_29

[9] L. Li, B. Shang, Y. Wu, J. Xiong, X. Chen, and Y. Xie, "Cyclops: A nanomaterial-based, battery-free intraocular pressure (IOP) monitoring system inside contact lens," in *Proc. 21st USENIX Symp. Netw. Syst. Design Implement. (NSDI)*, Apr. 2024, pp. 1659–1675. [Online]. Available: https://www.usenix.org/conference/nsdi24/presentation/li-liyao

[10] "Avery Dennison Smartrac DogBone RFID Paper Tag | M750," Accessed: Mar. 27, 2025. [Online]. Available: https://shorturl.at/PTZwB,

[11] "Packaged QFN or Bumped Die on Wafer—Axzon," Accessed: Mar. 27, 2025. [Online]. Available: https://www.axzon.com/packagedQFN.html

[12] J. Wang, O. Abari, and S. Keshav, "Challenge: RFID hacking for fun and profit," in *Proc. 24th Annu. Int. Conf. Mobile Comput. Netw.*, 2018, pp. 461–470. [Online]. Available: https://doi.org/10.1145/3241539.3241561

[13] M. Wagih, A. S. Weddell, and S. Beeby, "Battery-free wireless light-sensing tag based on a long-range dual-port dual-polarized RFID platform," *Sensors*, vol. 22, no. 13, p. 4782, 2022. [Online]. Available: https://www.mdpi.com/1424-8220/22/13/4782

[14] J. Zaid, A. Abdulhadi, A. Kesavan, Y. Belaizi, and T. Denidni, "Multiport circular polarized RFID-tag antenna for UHF sensor applications," *Sensors*, vol. 17, no. 7, p. 1576, Jul. 2017. [Online]. Available: http://dx.doi.org/10.3390/s17071576

[15] N. Bhat, A. Gupta, I. Bansal, H. Govindarajan, and D. Bharadia, "ZenseTag: An RFID assisted twin-tag single antenna cots sensor interface," in *Proc. 22nd ACM Conf. Embedded Netw. Sens. Syst.*, 2024, pp. 336–350. [Online]. Available: https://doi.org/10.1145/3666025.3699342

[16] I. Bansal, N. Bhat, A. Gupta, H. Govindarajan, and D. Bharadia, "SenSync: Real-time and accurate passive sensing," in *Proc. IEEE Int. Conf. RFID (RFID)*, 2025, pp. 1–6.

[17] J. Nolan, K. Qian, and X. Zhang, "KeyStub: A passive RFID-based keypad interface using resonant stubs," *Proc. ACM Interact. Mob. Wearable Ubiquitous Technol.*, vol. 7, no. 4, p. 173, Jan. 2024. [Online]. Available: https://doi.org/10.1145/3631442

[18] "Jadaktech," Accessed: Jun. 27, 2025. [Online]. Available: https://www.jadaktech.com/product/oem-fixed-mount-thingmagic-rfid-scanner-sargas-uhf-rain-jadak/

[19] *EPC^{TM} Radio-Frequency Identity Generation-2 V3 UHF RFID Standard*, Global Standards 1, 2024. [Online]. Available: https://ref.gs1.org/standards/gen2/

[20] M. Buettner and D. Wetherall, "A 'gen 2' RFID monitor based on the USRP," *SIGCOMM Comput. Commun. Rev.*, vol. 40, no. 3, pp. 41–47, Jun. 2010. [Online]. Available: https://doi.org/10.1145/1823844.1823850

[21] I. Bansal, N. Bhat, A. Gupta, H. Govindarajan, and D. Bharadia, "Demo abstract—SIGAR: Sensor integration gateway using augmented reality," in *Proc. 23rd ACM Conf. Embedded Netw. Sens. Syst.*, 2025, pp. 696–697. [Online]. Available: https://doi.org/10.1145/3715014.3724364

[22] "Wiliot platform—IoT pixel," Wiliot, 2024. [Online]. Available: https://www.wiliot.com/product/iot-pixels

[23] *Wirelessly Powered Sensor Networks and Computational RFID*.New York, NY, USA: Springer, 2013. [Online]. Available: http://dx.doi.org/10.1007/978-1-4419-6166-2

[24] G. Moloudian et al., "RF energy harvesting techniques for battery-less wireless sensing, industry 4.0, and Internet of Things: A review," *IEEE Sensors J.*, vol. 24, no. 5, pp. 5732–5745, Mar. 2024.

[25] X. Li et al., "ViPSN: A vibration-powered IoT platform," *IEEE Internet Things J.*, vol. 8, no. 3, pp. 1728–1739, Feb. 2021.

[26] N. Arora et al., "MARS: Nano-power battery-free wireless interfaces for touch, swipe and speech input," in *Proc. 34th Annu. ACM Symp. User Interface Softw. Technol.*, 2021, pp. 1305–1325. [Online]. Available: https://doi.org/10.1145/3472749.3474823

[27] C. Li, Z. Meng, Z. Li, N. Gao, Z. Zhang, and D. Zhen, "UHF RFID differential sensing via the backscatter coupling between the reader-tag antennas," *IEEE Sensors J.*, vol. 24, no. 13, pp. 21395–21408, Jul. 2024.

[28] G. Shi et al., "Analysis of mutual couple effect of UHF RFID antenna for the Internet of Things environment," *IEEE Access*, vol. 7, pp. 81451–81465, 2019.

[29] H. Cai et al., "When tags 'read' each other: Enabling low-cost and convenient tag mutual identification," *ACM Trans. Sen. Netw.*, vol. 18, no. 2, p. 22, Mar. 2022. [Online]. Available: https://doi.org/10.1145/3494541

[30] X. Zhang, H.-X. Li, and H. S.-H. Chung, "Setup-independent sensing architecture with multiple UHF RFID sensor tags," *IEEE Internet Things J.*, vol. 9, no. 2, pp. 1243–1251, Jan. 2022.

[31] T. Wu et al., "Backscatter sensing with single-tag path variation cancelling," in *Proc. IEEE Int. Symp. Circuits Syst. (ISCAS)*, 2024, pp. 1–5.

[32] T. Wang, S. Dai, Y. Liu, and T. T. Ye, "Battery-less sensing of body movements through differential backscattered RFID signals," *IEEE Sensors J.*, vol. 22, no. 9, pp. 8490–8498, May 2022.

[33] X. Liang, Y. Ma, C. Tian, Y. Han, and K. Liu, "Moc-SAR: Motion compensation for synthetic aperture-based holographic localization in UHF RFID system," *IEEE Sensors J.*, vol. 24, no. 19, pp. 30758–30768, Oct. 2024.

[34] C. Pfeiffer, "Fundamental efficiency limits for small metallic antennas," *IEEE Trans. Antennas Propag.*, vol. 65, no. 4, pp. 1642–1650, Apr. 2017.

[35] K. V. S. Rao, P. V. Nikitin, and S. F. Lam, "Antenna design for UHF RFID tags: A review and a practical application," *IEEE Trans. Antennas Propag.*, vol. 53, no. 12, pp. 3870–3876, Dec. 2005.

[36] H. Vogt, "Efficient object identification with passive RFID tags," in *Proc. 1st Int. Conf. Pervasive Comput.*, 2002, pp. 98–113.

[37] "NXP," Accessed: Feb. 9, 2025. [Online]. Available: https://www.nxp.com/docs/en/data-sheet/SL3ICS1002_1202.pdf .

[38] H. Sakoe and S. Chiba, "Dynamic programming algorithm optimization for spoken word recognition," *IEEE Trans. Acoust., Speech, Signal Process.*, vol. 26, no. 1, pp. 43–49, Feb. 1978.

[39] I. Bansal, "Sensync," 2025. [Online]. Available: https://github.com/ucsdwcsng/SenSync

[40] I. Bansal, N. Bhat, A. Gupta, H. Govindarajan, and D. Bharadia, "ZenseTag: An RFID assisted twin-tag single antenna cots sensor interface," in *Proc. 30th Annu. Int. Conf. Mobile Comput. Netw.*, 2024, pp. 1757–1759. [Online]. Available: https://doi.org/10.1145/3636534.3698850

[41] P. Nikitin, J. Kim, and K. Rao, "RFID tag analysis using an equivalent circuit," in *Proc. IEEE Int. Symp. Antennas Propag. USNC-URSI Radio Sci. Meeting (APS/URSI)*, 2021, pp. 167–168.

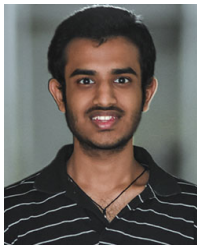

Ishan Bansal (Member, IEEE) received the B.E. degree in electronics and communication engineering from the Birla Institute of Technology and Science, Pilani, India, in 2020, and the M.S. degree in electrical and computer engineering from the University of California San Diego, USA, in 2025. He is currently pursuing the Ph.D. degree in electrical and computer engineering with UCSD, where he is a recipient of the Centaur Graduate Fellowship. He is a Graduate Student Researcher with the Wireless Communication, Sensing, and Networking Group, advised by Prof. D. Bharadia. Before graduate studies, he worked as a Senior Software Developer with Cisco Systems, Bengaluru, India, where he contributed to cloud infrastructure development and management. His research focuses on wireless and battery-free sensing platforms, RFID-based systems, and low-power signal processing for the Internet of Things. He is a recipient of the Best Paper Award at IEEE RFID 2025 and the Runner-Up Best Demo Awards at ACM MobiCom 2024 and ACM SenSys 2025.

Nagarjun Bhat (Graduate Student Member, IEEE) received the B.Tech. degree in electronics and communication engineering from Visvesvaraya Technological University, India, in 2014, and the M.S. degree in electrical and computer engineering from the University of Michigan at Ann Arbor, Ann Arbor, USA, in 2015. He is currently pursuing the Ph.D. degree in electrical and computer engineering with the Wireless Communication, Sensing, and Networking Group, University of California at San Diego, La Jolla. Before his Ph.D., he worked as an RF and Antenna Engineer with Laird Technologies, Motorola Mobility, Motorola Solutions, Pixxel Space, and Tesla, where he contributed to antenna and RF subsystem design for RFID systems, public safety radios, bezel-free smartphones, low-Earth-orbit satellites, and autonomous vehicles. He has co-authored publications in ACM SenSys, ACM MobiCom, IEEE RFID, *ACM on Interactive, Mobile, Wearable and Ubiquitous Technologies*, and the SmallSat Conference. His research focuses on passive and battery-free wireless sensing, including RFID-assisted sensor interfaces, differential passive sensing, reconfigurable intelligent surfaces, and wireless biomechanical sensing for healthcare applications. He is the recipient of the Best Student Paper Award at IEEE RFID 2025 (co-author), the Graduate Interdisciplinary Research Award at UC San Diego, and the Multiple Best Demo/Poster Awards at ACM SenSys, ACM MobiCom, and the UCSD ECE Research Expo.

Harine Govindarajan received the M.S. degree in electrical and computer engineering from the University of California San Diego, La Jolla, CA, USA, in 2025. Her research centers on applied electromagnetics and low-cost wireless sensing, spanning antenna design for satellite, wearable, and automotive applications, passive RFID sensing, and RF system development. She was a Research Intern with the University of Catania, Italy, where she designed and characterized a dual circularly polarized cross-dipole feed for L-band CubeSat reflectors, and an RF Engineering Intern with Skyworks Solutions, Irvine, CA, USA, where she worked on surface-acoustic-wave filter design for smartphone applications. She has coauthored work in IEEE ANTENNAS AND WIRELESS PROPAGATION LETTERS and ACM wireless conference proceedings.

Agrim Gupta received the Dual B.Tech. and M.Tech. degrees from the Indian Institute of Technology Bombay, India, where he worked on limited-feedback SVD precoding for MIMO-OFDM systems, and the Ph.D. degree in electrical and computer engineering from the University of California at San Diego (UCSD), La Jolla, CA, USA. His dissertation at UCSD was titled: "Sustainable Wireless Communications and Sensing," where he worked on energy-efficient wireless systems and scalable cellular network design, along with battery-free sensing and spectrum/operational-cost optimization. Notably, his research included ForceSticker—a batteryless wireless force/ubiquitous-weight sensing platform, and GreenMO—methods to sustainably scale multi antenna systems. He has co-authored publications in wireless communications and sensing domains across a diverse set of IEEE/ACM venues. His research interests include low-power backscatter sensing, green wireless networks, and network optimization for next-generation communications.

Dinesh Bharadia (Senior Member, IEEE) received the B.Tech. degree (with Gold Medal) in electrical engineering from the Indian Institute of Technology Kanpur, Kanpur, India, in 2010, and the Ph.D. degree from Stanford University. He is an Associate Professor with the Department of Electrical and Computer Engineering, University of California at San Diego (UCSD), with an affiliate appointment in the Computer Science and Engineering Department. His research leads the Wireless Communication, Sensing, and Networking Group, which explores systems spanning wireless communications, sensing, networking, vision, machine learning, and autonomous systems—building from theory to practical prototyping. During his Ph.D. he worked on full-duplex radios, enabling simultaneous transmission and reception on the same frequency—a foundational challenge in wireless systems. He also co-founded a company Kumu Networks, to commercialize full-duplex radio technology; in that role, he led architecture and algorithmic design, and oversaw field trials with Tier-1 operators, including Deutsche Telekom and SK Telecom. Among his honors, he was awarded the Klein-Gilhousen Chancellor's Endowed Chair at UCSD in 2023, Qualcomm Innovation Fellowships in 2020 and 2022, the Marconi Young Scholar Award, recognition as a Forbes 30 Under 30 in Science as well as the MIT Technology Review 35 under 35.